Design and Mathematical Modeling of a Novel Angular Displacement Transformer for Accurate Diagnostics of Angular Displacements

Amirov Sulton Fayzullayevich[1]
[1]Department of Electricity Supply, Tashkent State Transport University, 100167
Temiryulchilar-1 str., Tashkent Uzbekistan
[1]amirov_s@tstu.uz (https://orcid.org/0000-0001-7212-3438)

Mamadaliyev Ulugbek Shukhratovich[2]
[2]Department of Electrical enginer, Tashkent State Transport University, 100167
Temiryulchilar-1 str., Tashkent Uzbekistan
[2]mamadaliyev_u@tstu.uz (https://orcid.org/0009-0007-3337-5692)

Bayanov Ildar Nazipovich[3]
[3]Department of Electrical enginer, Tashkent State Transport University, 100167
Temiryulchilar-1 str., Tashkent Uzbekistan
[3]bayanov_i@tstu.uz (https://orcid.org/0000-0003-3645-084X)

ABSTRACT

This paper investigates the linear and nonlinear distributed-parameter circuits of a new resonant electromagnetic transducer intended for converting motion parameters (displacement and velocity) into electrical signals. It is shown that in the linear distributed-parameter circuit of the transducer, the magnetic flux and magnetic field intensity vary along the length of the circuit according to a nonlinear law; moreover, the degree of this nonlinearity increases with an increase in the attenuation coefficient of the magnetic field along the magnetic circuit. When the distributed-parameter magnetic circuit of the transducer operates in the nonlinear regime, achieving a linear distribution of the working magnetic flux along the circuit length requires that the working air gap between adjacent long ferromagnetic rods vary along the length of the circuit according to a prescribed law. In this case, the magnitude of the variation of the working magnetic flux along the circuit length does not depend on the value of the approximation coefficient characterizing the nonlinearity of the circuit.

Keywords:

angular displacement transformer (ADT), movable ferromagnetic core, E-shaped magnetic core, horseshoe-shaped magnetic core, magnetic circuit, electromotive force (EMF), magnetic flux, linear diagnostics characteristic, differential transformer, distributed-parameter model, diagnostics range, excitation and diagnostics coils, spiral-shaped ferromagnetic core, static characteristics, sensitivity

1 INTRODUCTION

Electromagnetic converters, in particular, transformer converters are widely used for obtaining reliable information about the angular movements of controlled objectsin automatic control systems and management of various technological and production processes [1, 2]. Compared with other types of angular displacement converters, they have high reliability and stable metrological characteristics in extreme operating conditions [3, 4]. At the same time, they have a relatively low sensitivity and a nonlinear static characteristic [5].

In this article, research is carried out on the development of transformer-based angular displacement transducers characterized by high sensitivity, a simple structure, high output power, and a linear conversion function. In addition, the study focuses on the design of new transformer transducer configurations intended for monitoring and control systems of technological processes, as well as on improving methods for their calculation.

New differential type ADT converters have been developed [6, 7] at the "Power Supply" Department of the Tashkent State Transport University, the design scheme of one of them is shown in Fig.1.

2 METHODS

This study employed an integrated approach to analyze and develop a new ADT.

Design and Modeling: Two types of magnetic cores (horseshoe and O-/E-shaped) were developed, with optimized movable ferromagnetic cores and excitation/sensing coils to ensure high sensitivity, linear output, and simple construction.

Mathematical Modeling: Differential equations based on Kirchhoff's laws were formulated to describe the magnetic circuits. Flux and EMF were analyzed as functions of angular displacement, and solutions under boundary conditions enabled calculation of output signals [8].

Experimental Verification: Laboratory tests of ADT prototypes assessed linearity, repeatability, and diagnostics range. Comparison with theoretical predictions showed differences of 3.5–5.5%, confirming model reliability.

Optimization: Core surface characteristics and design parameters were analyzed to expand diagnostics range and achieve linear static response.

Overall, the methods combined design, mathematical modeling, and experimental validation to evaluate the ADT performance comprehensively.

3 RESEARCH RESULTS

The ADT comprises two horseshoe-shaped movable magnetic cores, formed as open rings bounded by curved lines following an Archimedean spiral, and two vertically aligned magnetic cores arranged in alternating and opposite positions at specific intervals. The thickness of these cores increases linearly with the angular coordinate, resulting in working surfaces that vary proportionally with angular displacement.

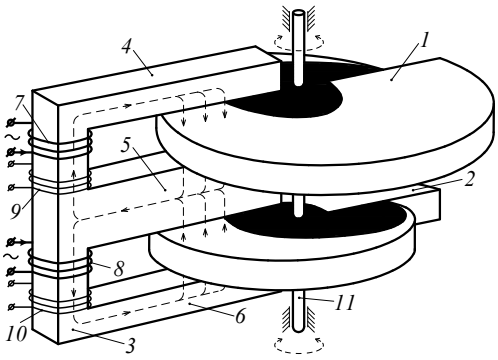

Figure 1. Schematic design of the novel ADT: 1, 2 – movable horseshoe-shaped magnetic cores; 3, 4, 5, 6 – vertical base and mutually parallel rods of the E-shaped fixed magnetic core; 7, 8 – excitation coil sections; 9, 10 – diagnostics coil sections; 11 – shaft

Magnetic core 1 is positioned between the upper two adjacent rods (4 and 5) of an E-shaped core assembly with three parallel and radially arranged rods mounted on a vertical stem (3), while magnetic core 2 is placed between the lower two rods (5 and 6) of the same E-shaped assembly, allowing relative movement. The vertical stem (3) supports two excitation coil sections (7 and 8) and two diagnostics coil sections (9 and 10), each connected in series and wound in opposite directions inductively. The ends of the vertical stem are mechanically coupled to the monitored object via corresponding semi-arms (11 and 12) to control angular displacement [9, 10].

The ADT operates as follows. The excitation coil is connected to a sinusoidal current source. As this current passes through the sections of the excitation coil, it generates magneto motive forces (MMF) in the wound rod 3, with a magnitude $F_e = I_e w_e$, where w_e and I_e are the number of turns in the excitation coil section and the current passing through it, respectively. Under the influence of these MMFs, the corresponding sections of the magnetic circuit produce sinusoidally varying magnetic fluxes $Q_{\mu 1}$ and $Q_{\mu 2}$.

In the neutral position of the movable part (MP) of the ADT (Fig. 1), the magnetic reluctances of the working air gaps between magnetic core 1 and the E-shaped core rods 4 and 5, as well as between magnetic core 2 and rods 5 and 6, are expressed as $W_{\mu\delta_w 1} = \frac{2\delta_w}{\mu_0 S_{\mu\delta_w 1}(\alpha)}, [H^{-1}]$ and $W_{\mu\delta_w 2} = \frac{2\delta_w}{\mu_0 S_{\mu\delta_w 2}(\alpha)}, [H^{-1}]$, where $S_{\mu\delta_w 1}(\alpha), [m^2]$ and $S_{\mu\delta_w 2}(\alpha), [m^2]$ are the effective areas of the working air gaps. According to the energy–information model for chains of mechanical, electrical, magnetic, and other physical nature [11] (and using the classical analogy where magnetic reluctance corresponds to resistance), these values are equal due to the equality of the effective areas of the air gaps. Consequently, the magnetic fluxes through these gaps are also equal:

$$Q_{\mu 1} = F_e \frac{\mu_0 S_{\mu\delta_w 1}(\alpha)}{2\delta_w}, [Wb],$$

$$Q_{\mu 2} = F_e \frac{\mu_0 S_{\mu\delta_w 2}(\alpha)}{2\delta_w}, [Wb].$$

As a result, the net EMF in the diagnostics coil, which consists of two sections connected in series but inductively opposed (differential scheme), becomes zero.

In the new ADT, the MP can be implemented either as two horseshoe-shaped movable magnetic cores forming a continuous loop or as an E-shaped fixed magnetic core. The movable horseshoe magnetic cores are rigidly attached to the monitored object via a shaft. When the movable cores rotate by an angle α in a given direction (e.g., counterclockwise), the effective active area of the air gap between rods 4 and 5 and magnetic core 1, $S_{\mu\delta_w 1}(\alpha)$ increases linearly according to the law

$$S_{\mu\delta_w 1}(\alpha) = \frac{ba}{\pi}(\alpha_м + \alpha)$$

(due to the thicker part of core 1 entering the gap as the MP rotates; see Fig. 2a, rods 4 and 5 shown by dashed lines). Consequently, the magnetic flux passing through this area, $Q_{\mu 1}$, increases.

Conversely, the effective active area of the air gap between rods 5 and 6 and magnetic core 2, $S_{\mu\delta_w 2}(\alpha)$, decreases linearly according to

$$S_{\mu\delta_w 2}(\alpha) = \frac{ba}{\pi}(\alpha_м - \alpha)$$

(due to the thinner part of core 2 entering the gap; see Fig. 2b, rods 5 and 6 shown by dashed lines), which reduces the magnetic flux $Q_{\mu 2}$.

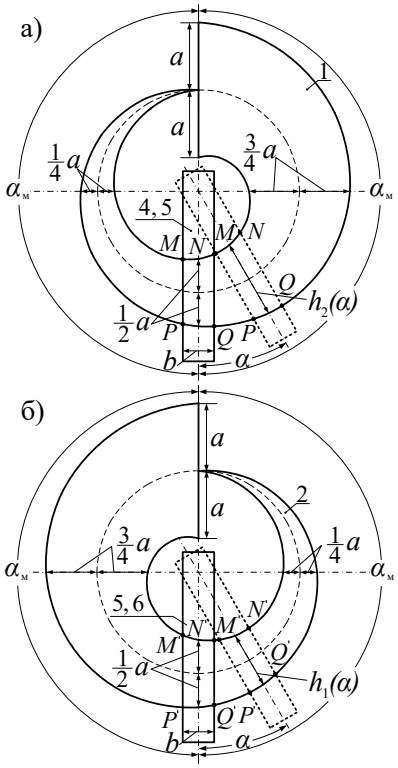

Figure 2. Diagrams for determining the analytical expressions of the effective areas formed between the E-shaped magnetic core rods 4 and 5 and magnetic core 1 (a), as well as between rods 5 and 6 and magnetic core 2 (b), in the new ADT, as functions of the measured angular displacement coordinate

As a result, electromotive forces (EMFs) proportional to the magnetic flux in each section of the diagnostics coil are induced. Since the coil sections are connected in series but in opposite inductive directions (i.e., a differential configuration), the coil output produces a differential signal proportional to the change in magnetic flux, and hence to the angular displacement of the MP, i.e.,

$$\dot{E}_{out} = -(\dot{E}_1 - \dot{E}_2) = -j\omega \dot{I}_e w_e w_{out} \mu_0 \frac{ba}{\pi \delta_w} \alpha. \quad (1)$$

In the novel ADT, the MP of the horseshoe-shaped core (comprising the winding, ferromagnetic core, and electromagnetic screen) moves between the corresponding rods of the E-shaped magnetic core. The effective area formed between these rods by the MP, which determines the measured angular displacement, is analytically expressed as a

function of the angular displacement coordinate (see Figures 2–6).

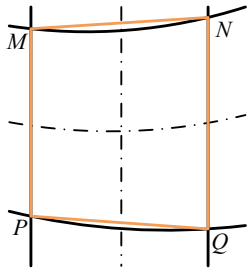

Figure 3. Area of the MNPQ trapezoid

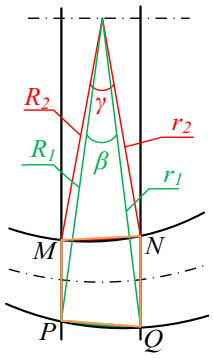

Figure 4. Diagram for determining the areas $S_{\mu 1}(\alpha)$ (red) and $S_{\mu 2}(\alpha)$ (green)

From the diagrams in Figures 2–6, the following expressions for the active area of the MP can be written [12, p. 128]:

$$S_{\mu\delta_w 1\Sigma}(\alpha) = S_{\mu\delta_w 1}(\alpha) + S_{\mu 1}(\alpha) - S_{\mu 2}(\alpha) = \\ = \frac{ba}{\pi}(\alpha_{\text{м}} + \alpha) + \frac{R_1 r_1}{2}\left(\frac{\beta\pi}{180} - sin\beta\right) - \\ - \frac{R_2 r_2}{2}\left(\frac{\gamma\pi}{180} - sin\gamma\right), \quad (2)$$

where, $S_{\mu\delta_w 1}(\alpha) = \frac{ba}{\pi}(\alpha_{\text{м}} + \alpha)$ – the area of the MNPQ trapezoid; $S_{\mu 1}(\alpha) = \frac{R_1 r_1}{2}\left(\frac{\beta\pi}{180} - sin\beta\right)$ – the area of the ferromagnetic core contour bounded by the PQ side and the PQ arc of the MNPQ trapezoid (Figs. 2a, 3, and 4); $S_{\mu 2}(\alpha) = \frac{R_2 r_2}{2}\left(\frac{\gamma\pi}{180} - sin\gamma\right)$ – the area of the ferromagnetic core contour bounded by the MN side and the MN arc of the MNPQ trapezoid (Figs. 2a, 3, and 4); R_1, r_1, R_2, r_2 are the radii, and β, γ are the angles, as shown in Fig. 4.

$$S_{\mu\delta_w 2\Sigma}(\alpha) = S_{\mu\delta_w 2}(\alpha) + S'_{\mu 1}(\alpha) - S'_{\mu 2}(\alpha) = \\ = \frac{ba}{\pi}(\alpha_{\text{м}} - \alpha) + \frac{R'_1 r'_1}{2}\left(\frac{\beta'\pi}{180} - sin\beta'\right) - \\ - \frac{R'_2 r'_2}{2}\left(\frac{\gamma'\pi}{180} - sin\gamma'\right), \quad (3)$$

where, $S_{\mu\delta_w 2}(\alpha) = \frac{ab}{\pi}(\alpha_{\text{м}} - \alpha)$ - the area of the M′N′P′Q′ trapezoid; $S'_{\mu 1}(\alpha) = \frac{R'_1 r'_1}{2}\left(\frac{\beta'\pi}{180} - sin\beta'\right)$ - the area of the ferromagnetic core contour of the M′N′P′Q′ trapezoid bounded by the P′Q′ side and the P′Q′ arc (Figures 2b, 5, and 6); $S'_{\mu 2}(\alpha) = \frac{R'_2 r'_2}{2}\left(\frac{\gamma'\pi}{180} - sin\gamma'\right)$ - the area of the ferromagnetic core contour of the M′N′P′Q′ trapezoid bounded by the M′N′ side and the M′N′ arc (Figures 2b, 5, and 6); the radii R'_1, r'_1, R'_2, r'_2 and the angles β', γ' are shown in Figure 6.

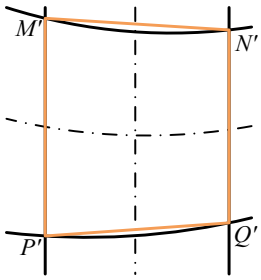

Figure 5. Area of the $M'N'P'Q'$ trapezoid

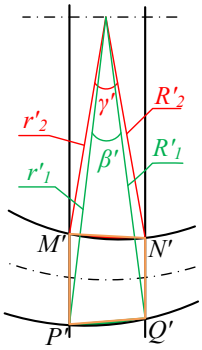

Figure 6. Diagram for determining the areas $S'_{\mu 1}(\alpha)$ (red) and $S'_{\mu 2}(\alpha)$ (green)

The analysis of the determined values of the components forming $S_{\mu\delta_w 1\Sigma}(\alpha)$ for the specific values of $R_1, r_1, R_2, r_2, \beta, \gamma$, and α as well as $S_{\mu\delta_w 2\Sigma}(\alpha)$ for the specific values of $R'_1, r'_1, R'_2, r'_2, \beta', \gamma'$, and α shows that in equations (2) and (3) the differences on the right-hand side, namely $\Delta S = S_{\mu 1}(\alpha) - S_{\mu 2}(\alpha)$ and $S'_{\mu 1}(\alpha) - S'_{\mu 2}(\alpha)$, do not exceed 0.333% of the corresponding values of $S_{\mu\delta_w 1}(\alpha)$ and $S_{\mu\delta_w 2}(\alpha)$. Therefore, these differences on the right-hand side of equations (2) and (3) can be neglected, and the equations can be expressed in the simplified form as follows:

$$S_{\mu\delta_w 1\Sigma}(\alpha) \approx S_{\mu\delta_w 1}(\alpha) = \frac{ba}{\pi}(\alpha_{\text{м}} + \alpha), \quad (4)$$

$$S_{\mu\delta_w 2\Sigma}(\alpha) \approx S_{\mu\delta_w 2}(\alpha) = \frac{ba}{\pi}(\alpha_{\text{м}} - \alpha). \quad (5)$$

The expressions obtained in (2.4) and (2.5) indicate the linear relationship between the active area of the MP of the new ADT and the measured quantity.

In analyzing the magnetic circuit of the investigated new ADT, whose MP consists of a ferromagnetic core, the following two cases are considered: 1. The magnetic flux in the air gap between the two adjacent long and mutually parallel rods of the E-shaped magnetic core is assumed to be zero (since this air gap δ_s is significantly larger than the working air gap δ_w, i.e., $\delta_s \gg \delta_w$, so ($C_{\mu sp} \approx 0$), while in the portion of the magnetic circuit containing the movable core, the parameters are $Z_{\mu p} = const$ and

$Y_{\mu w.p} = \frac{1}{\sqrt{\left(\frac{1}{C_{\mu w}}\right)^2 + Z_{\mu cp.}^2 \cdot X_м}} = const$ (where, $C_{\mu w} = \mu_0 \frac{bX_м}{2\delta_w}$, $[H]$ — the magnetic capacitance of the working air gaps between the E-shaped core rods and the active surface of the movable spiral-shaped ferromagnetic core; $Z_{\mu cp}$, $[H^{-1}]$ — the total magnetic reluctance along the working flux path of the active portion of the spiral-shaped ferromagnetic core), these parameters are considered distributed; 2. The parameters $Z_{\mu p} = const$, $C_{\mu sp} = const$, $Z_{\mu w.p} = const$ and $Y_{\mu w.p} = const$ are assumed to be distributed.

For the first case, the magnetic circuit is analyzed. The upper half of the ADT is shown in Fig. 1, while the structural diagram of the magnetic circuit for the configuration in Fig. 2(a) is presented. The equivalent circuit of its elementary section of length dx_1 is illustrated in Fig. 7(a, b) [13,14].

In the calculations, the investigated magnetic circuit is represented as a Π -shaped magnetic core with long parallel rods, where the width of its working air gap (2x) along the rod length is modeled as a spiral-shaped ferromagnetic core whose dimension varies linearly with the angular displacement coordinate.

For the elementary segment dx_1 of this magnetic circuit, the differential equations derived based on Kirchhoff's laws are expressed as follows (Fig. 7 b):

$$Q'_{\mu x_2} = -U_{\mu x_2} Y_{\mu w.p}, \quad (6)$$

$$U'_{\mu x_2} = -2Z_{\mu w.p} Q_{\mu x_2}, \quad (7)$$

where $Z_{\mu p} = \frac{1}{\mu\mu_0 bh}$, $[H^{-1} \cdot m^{-1}]$; $Y_{\mu w.p}$, $[H \cdot m^{-1}]$ - E-shaped magnetic core rods' magnetic reluctance, the reluctance of the movable ferromagnetic core with variable active surface, and the per-unit value of the magnetic flux in the working air gaps between these rods.

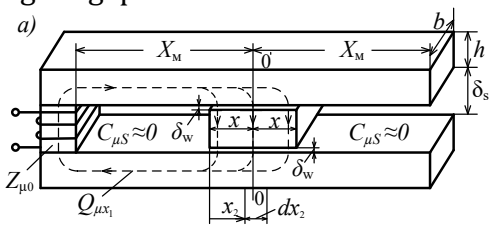

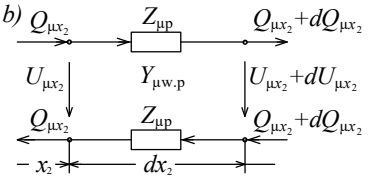

Figure 7. Structural (a) and equivalent circuit (b) diagrams of the magnetic circuit of the novel ADT with a movable ferromagnetic core of variable active surface and its elemental segment of length dx_1

The general solution of the differential equations (6) and (7) can be expressed as follows:

$$Q_{\mu x_2} = A_1 e^{\gamma_w x_2} + A_2 e^{-\gamma_w x_2}, \quad (8)$$

$$U_{\mu x_2} = -A_1 \frac{\gamma_w}{Y_{\mu w.p}} e^{\gamma_w x_2} + A_2 \frac{\gamma_w}{Y_{\mu w.p}} e^{-\gamma_w x_2}, \quad (9)$$

where, $\gamma_w = \sqrt{2Z_{\mu p} Y_{\mu w.p}}$, $[m^{-1}]$.

The integration constants A_1 and A_2 are determined based on the following boundary conditions appropriate for the magnetic circuit under study:

$$U_{\mu x_2 = 0} = F_e - Q_{\mu x_2 = 0}\left[Z_{\mu 0} + 2Z_{\mu p}(X_м - x)\right];$$
$$Q_{\mu x_2 = 2x} = 0, \quad (10)$$

By substituting the boundary values of $Q_{\mu x_1}$ and $U_{\mu x_1}$ into expressions (10) and solving the resulting system of algebraic equations for the unknowns A_1 and A_2, we obtain the following values:

$$A_1 = -\frac{F_e}{2\Delta_4} e^{-2\gamma_w x}; \quad A_2 = \frac{F_e}{2\Delta_4} e^{2\gamma_w x}, \quad (11)$$

where, $\Delta_4 = \left[Z_{\mu 0} + 2Z_{\mu p}(X_м - x)\right] sh(2\gamma_w x) + \frac{\gamma_w}{Y_{\mu w.p}} ch(2\gamma_w x)$, $[H^{-1}]$.

From the obtained values of A_1 and A_2, the following values of $Q_{\mu x_1}$ and $U_{\mu x_1}$ are obtained:

$$Q_{\mu x_1} = \frac{F_e}{\Delta_4} sh[\gamma_w(2x - x_2)], \quad (12)$$

$$U_{\mu x_2} = -\frac{F_e}{\gamma_w \Delta_4} ch[\gamma_w(2x - x_2)]. \quad (13)$$

For the first case under consideration, the magnetic flux and EMF generated in the measuring coil of the novel ADT are determined as follows, taking into account $x = \frac{a}{2\pi}(\alpha_м + \alpha)$ and $X_м = \frac{a}{\pi}\alpha_м$

$$Q_{\mu\alpha}^{up} = Q_{\mu x_2 = 0} = \frac{\dot{F}_e}{2\Delta_{41}^*} sh[\beta_w(1 + \alpha^*)], \quad (14)$$

$$\dot{E}_{out9} = -j\omega w_{out} \frac{\dot{F}_e}{2\Delta_{41}^*} sh[\beta_w(1 + \alpha^*)], \quad (15)$$

where, $\Delta_{41}^{*}=\left[Z_{\mu 0}+Z_{\mu}(1-\alpha^{*})\right]sh[\beta_w(1+\alpha^{*})]+\frac{\beta_w}{Y_{\mu w.p}}ch[\beta_w(1+\alpha^{*})],[H^{-1}]$; $\beta_w=\gamma_w\frac{a}{\pi}\alpha_{\text{м}}=\gamma_w X_{\text{м}},[m^{-1}]$; $Z_{\mu}=Z_{\mu p}X_{\text{м}},[H^{-1}]$; $Y_{\mu w}=Y_{\mu w.p}X_{\text{м}},[H]$.

Similarly, for the lower half of the ADT shown in Fig. 1 and for the configuration in Fig. 2b, by performing the calculations in the same manner as above, we obtain the following expressions for the magnetic flux and EMF generated in the measuring coil of the novel ADT:

$$Q_{\mu\alpha}^{low}=Q_{\mu x_1=0}=\frac{F_e}{2\Delta_4}sh\left[\gamma_w\frac{a}{\pi}(\alpha_{\text{м}}-\alpha)\right]=$$
$$=\frac{\dot{F}_e}{2\Delta_{42}^{*}}sh[\beta_w(1-\alpha^{*})]. \quad (16)$$

$$\dot{E}_{out10}=-j\omega w_{out}\dot{Q}_{\mu\alpha}^{low}=$$
$$=-j\omega w_{out}\frac{\dot{F}_e}{2\Delta_2}sh[\beta_w(1-\alpha^{*})], \quad (17)$$

where, $\Delta_{42}^{*}=\left[Z_{\mu 0}+Z_{\mu}(1+\alpha^{*})\right]sh[\beta_w(1-\alpha^{*})]+\frac{\beta_w}{Y_{\mu w}}ch[\beta_w(1-\alpha^{*})],[H^{-1}]$.

Figure 8 presents the graphs of the functions $Q_{\mu\alpha}^{up*}=f(\alpha^{*})$ and $Q_{\mu\alpha}^{low*}=f(\alpha^{*})$ for different values of β_w. The analysis of these graphs demonstrates that the relationship between the working magnetic flux and the angular coordinate of the MP remains linear across various β_w values. The discrepancy between the calculated and experimental results did not exceed 3.5–5.5%. It is noteworthy that, in the prototype of the novel ADT, the β_w value was adjusted solely by changing the relative magnetic permeability of the ferromagnetic material.

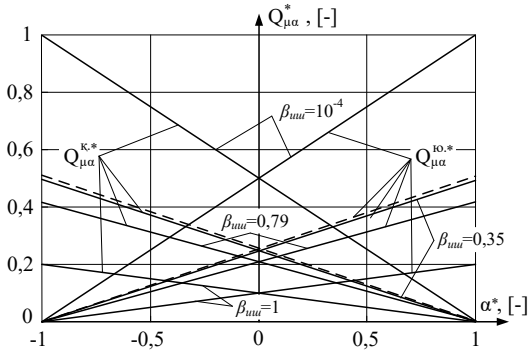

Figure 8. Graphs of the functions $Q_{\mu\alpha}^{up*}=f(\alpha^{*})$ and $Q_{\mu\alpha}^{low*}=f(\alpha^{*})$ for various values of β_w

Now, we proceed to calculate the magnetic circuit for the second case. The upper half of the ADT shown in Figure 1 and the structural scheme of the magnetic circuit depicted in Figure 2(a) are considered. The corresponding schemes for its elementary sections of lengths dx_1, dx_2 and dx_3 are presented in Figures 9(b–d) [15, 16].

For the elementary sections of this magnetic circuit, the differential equations formulated on the basis of Kirchhoff's laws can be written in the following form (Fig. 3.6, b–d):

$$Q'_{\mu x_1}=-U_{\mu x_1}C_{\mu sp}, \quad (18)$$
$$U'_{\mu x_1}=-2Z_{\mu p}Q_{\mu x_1}, \quad (19)$$
$$Q'_{\mu x_2}=-U_{\mu x_2}Y_{\mu w.p}, \quad (20)$$
$$U'_{\mu x_2}=-2Z_{\mu w.p}Q_{\mu x_2}, \quad (21)$$
$$Q'_{\mu x_3}=-U_{\mu x_3}C_{\mu sp}, \quad (22)$$
$$U'_{\mu x_3}=-2Z_{\mu p}Q_{\mu x_3}. \quad (23)$$

The general solutions of the differential equations (18), (19), (20), (21), as well as (22) and (23), are respectively given as follows:

$$Q_{\mu x_1}=A_1e^{\gamma_s x_1}+B_1e^{-\gamma_s x_1}, \quad (24)$$
$$U_{\mu x_1}=-A_1\frac{\gamma_s}{C_{\mu pp}}e^{\gamma_s x_1}+B_1\frac{\gamma_s}{C_{\mu pp}}e^{-\gamma_s x_1}, \quad (25)$$
$$Q_{\mu x_2}=A_2e^{\gamma_w x_2}+B_2e^{-\gamma_w x_2}, \quad (26)$$
$$U_{\mu x_2}=-A_2\frac{\gamma_w}{Y_{\mu w}}e^{\gamma_w x_2}+B_2\frac{\gamma_w}{Y_{\mu w}}e^{-\gamma_w x_2}, \quad (27)$$
$$Q_{\mu x_3}=A_3e^{\gamma_s x_3}+B_3e^{-\gamma_s x_3}, \quad (28)$$
$$U_{\mu x_3}=-A_3\frac{\gamma_s}{C_{\mu sp}}e^{\gamma_s x_3}+B_3\frac{\gamma_s}{C_{\mu sp}}e^{-\gamma_s x_3}. \quad (29)$$

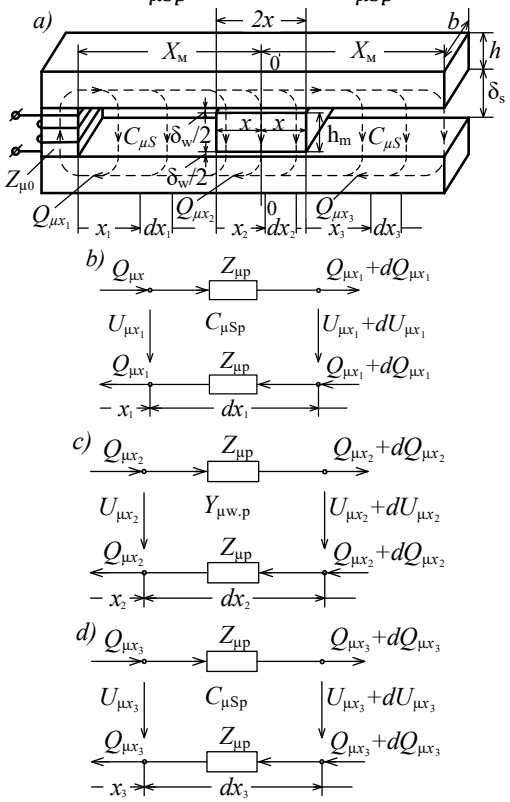

Figure 9. Constructive scheme of the magnetic circuit of the novel ADT with a movable ferromagnetic core for Case 2 (a) and equivalent circuits of its elemental sections with lengths dx_1 (b), dx_2 (c) and dx_3 (d)

For the magnetic circuit under investigation, the following boundary conditions apply:

$$U_{\mu x_1=0} = F_{к} - Q_{\mu x_1=0} Z_{\mu 0},\quad U_{\mu x_1=X_м - x} = U_{\mu x_2=0},$$
$$Q_{\mu x_1=X_м - x} = Q_{\mu x_2=0},\quad U_{\mu x_2=2x} = U_{\mu x_3=0},$$
$$Q_{\mu x_2=2x} = Q_{\mu x_3=0},\quad Q_{\mu x_3=X_м - x} = 0.$$

By substituting the boundary values of the magnetic fluxes and magnetic potentials into the corresponding equations and solving the resulting system with respect to the unknowns $A_1 \div A_3$ and $B_1 \div B_3$, their values were determined. Substituting the obtained values of $A_1 \div A_3$ and $B_1 \div B_3$ into equations (24)–(29), the expressions for the magnetic fluxes and magnetic potentials were derived [17, 18].

For the second case under consideration, the value of the magnetic flux that induces an EMF in the measuring winding of the new transformer measuring transducer with a ferromagnetic core is determined as follows, taking into account $x = \frac{a}{2\pi}(\alpha_м + \alpha)$ and $X_м = \frac{a}{\pi}\alpha_м$:

$$Q_{\mu x_1=0} = Q_{\mu\alpha}^{up} = \frac{8F_e}{C_{\mu sп} Y_{\mu w.p}^2 \Delta_{51}^*} \cdot$$
$$\cdot \left\{ \gamma_s^2 Y_{\mu w.p}^2 sh^2\left[\frac{1}{2}\beta_s(1-\alpha^*)\right] sh[\beta_w(1+\alpha^*)] + \right.$$
$$+\gamma_s^2 Y_{\mu w.p} ch^2\left[\frac{1}{2}\beta_s(1-\alpha^*)\right] sh[\beta_w(1+\alpha^*)] +$$
$$\left. + \frac{1}{2}\gamma_s\gamma_w\left(C_{\mu sп} + Y_{\mu w.p}\right) sh[\beta_w(1-\alpha^*)] \cdot \right.$$
$$\left. \cdot ch[\beta_w(1+\alpha^*)] \right\},$$

where, Δ_{51}^* differs from the expression Δ_5 by substituting $\frac{a}{2\pi}(\alpha_м + \alpha)$ instead of x, and $\frac{a}{\pi}\alpha_м$ instead of $X_м$.

By performing calculations analogous to those described above for the lower half of the transformer measuring transducer shown in Fig. 1 and for the structure presented in Fig. 2(b), the following expression is obtained for the value of the magnetic flux that induces the EMF in the measuring winding of the new transformer measuring transducer:

$$Q_{\mu\alpha}^{low} = \frac{8F_e}{C_{\mu sp} Y_{\mu w.p}^2 \Delta_{52}^*} \left\{ \gamma_s^2 Y_{\mu w.p}^2 sh^2\left[\frac{1}{2}\beta_s(1+\alpha^*)\right] \right.$$
$$\cdot sh[\beta_w(1-\alpha^*)] + \gamma_s^2 Y_{\mu w.p} ch^2\left[\frac{1}{2}\beta_s(1+\alpha^*)\right] \cdot$$
$$\cdot sh[\beta_w(1-\alpha^*)] + \frac{1}{2}\gamma_s\gamma_w\left(C_{\mu sp} + Y_{\mu w.p}\right) \cdot$$
$$\left. \cdot sh[\beta_w(1+\alpha^*)] ch[\beta_w(1-\alpha^*)] \right\},$$
$$\dot{E}_{out9} = -j\omega w_{out} \dot{Q}_{\mu\alpha}^{up};\quad \dot{E}_{out10} = -j\omega w_{out} \dot{Q}_{\mu\alpha}^{low}.$$

where, Δ_{52}^* differs from the expression Δ_5 by substituting $\frac{a}{2\pi}(\alpha_м - \alpha)$ instead of x, and $\frac{a}{\pi}\alpha_м$ instead of $X_м$.

The graphs of the functions $Q_{\mu\alpha}^{up*} = f(\alpha^*)$ and $Q_{\mu\alpha}^{low*} = f(\alpha^*)$, plotted for different values of β, do not differ qualitatively from the graphs shown in Fig. 8.

4 CONCLUSIONS

In the new ADT, arranging the movable magnetic cores as two horseshoe-shaped rings along a single vertical axis with a certain air gap in a staggered and oppositely positioned manner, where their active surfaces vary linearly with the angular coordinate, and designing the fixed magnetic cores in an E-shaped configuration, while positioning the horseshoe-shaped cores to move between each pair of parallel rods of the E-shaped magnetic core, and placing the excitation and measuring windings as two series-connected, inductively opposing sections based on the E-shaped core, allows the transformer to achieve an extended diagnostics range and ensures linearity of the transfer function across the full diagnostics range. The diagnostics range of the new ADT is approximately ±175 degrees.

Thus, the analysis of the newly proposed ADT presented above shows that the designed transformers have a wide diagnostics range, and their static characteristics exhibit a linear form, which is essential for the control and monitoring systems in which they are applied.

REFERENCES

[1] Ageikin D.I., Kostina E.N., Kuznetsova N.N. Sensors of control and regulation: reference materials / 2nd ed., reprint. and add. (inrussian) – Moscow: Mashinostroenie, 1965. – 928 p.

[2] Yusupbekov N.R., Igamberdiev H.Z., Malikov A.V. Fundamentals of automation of technological processes: A textbook for higher and secondary special education. In

2chapters (in russian) – Tashkent: TSTU, 2007. part 1, 2. – 152 p., 173 p.
[3] Zaripov M.F. Converters with distributed parameters for automation and information and diagnostics technology (in russian). Moscow, Energiya, 1969, 177 p.
[4] Fedotov A.V. Theory and calculation of inductive displacement sensors for automatic control systems: monograph (in russian) /. - Omsk: Publishing House of OmSTU, 2011. - 176 p.
[5] Konyukhov N.E., Mednikov F.M., Nechaevsky M.L. Electromagnetic sensors of mechanical quantities (in russian). – Moscow: Mashinostroenie, 1987. – 256 p.
[6] Patent of the Republic of Uzbekistan (UZ) No. IAP 06642. Transformer converter of angular displacements / Amirov S.F., Yuldashev N.R., FayzullaevJ.S., Jumaboev S.H. // Formal Bulletin, 2021. - No. 12.
[7] Application for the patent of the Republic of Uzbekistan (UZ) No. IAP 20220111. Transformer converter of angular displacements / Amirov S.F., Karimov I.A., Yuldashev N.R., Mamadaliev U.S., Shoimkulov A.A.// Date of application: 11.03.2022.
[8] Bul B.K. Fundamentals of the theory and calculation of magnetic circuits. - Moscow: Energy, 1964. - 464 p.
[9] Atabekov G.I. Theoretical foundations of electrical engineering. Linear electrical chains: A textbook. 7th ed. (in russian). – St. Petersburg: Publishing House "Lan", 2009. – 592 p.
[10] Patent of the Republic of Uzbekistan (UZ) No. IAP 07683. Angular Displacement Transducer / S. F. Amirov, I. A. Karimov, N. R. Yuldashev, U. Sh. Mamadaliev, A. A. Shoimqulov // Official Bulletin, 2024, No. 5.
[11] Amirov S. F., Mamadaliev U. Sh., Sulliev A. Kh. Flux Distribution in the Magnetic Circuits of Angular Displacement Transducers with a Variable Active Area of the Movable Core // Chemical Technology. Control and Management. – 2023, No. 5 (113). – pp. 22–31. (05.00.00; No. 12). https://ijctcm.researchcommons.org/journal/vol2023/iss5/4/
[12] Bronshtein I. N., Semendyaev K. A. Handbook of Mathematics for Engineers and University Students, 13th revised edition – Moscow: Nauka, Main Editor: Phys.-Math. Literature, 1986. – 544 p.
[13] A.s. No. 147108. Differential transformer sensor of large linear displacements of increased sensitivity / Chernov S.E., Kulikovskiy L.F., Zaripov M.F. // Bulletin of inventions, 1962. - No. 9.
[14] Demirchyan K.S., Neiman L.R., Korovkin N.V., Chechurin V.L. Theoretical foundations of electrical engineering: In 3 volumes. Textbook for universities. Ed. 4th - St. Petersburg: Peter, 2006. - volume 2. - p. 576 p.).
[15] Amirov S. F., Mamadaliev U. Sh., Karimov I. A., Sattorov T. A. Mathematical Models of Transformer Angular Displacement Transducers with a Variable Active Area of the Excitation Winding // Scientific-Technical Journal “Development of Science and Technology” of Bukhara Engineering Technology Institute, 2023, No. 6, pp. 197–205. (Resolution of the OAK Board dated 29.03.2017, No. 239/5).
[16] S.Amirov, A.Sulliev, S.Sharapov. Study on differential transformer displacement sensors. E3S Web of Conferences, 434, 02011, (2023), https://doi.org/10.1051/e3sconf/202343402011
[17] Rachkov M.Y. Technical means of automation. Textbook for high schools. - Moscow: MGIU, 2006. - 185 p.
[18] S.Amirov, A.Sulliev, U.Mukhtorov. Resonance sensors of motion parameters. AIP Conference Proceedings, 3256(1), 050028, (2025). https://doi.org/10.1063/5.0267548